*Research Report*

# Intercalation Electrode Materials Based on a Metal-organic Framework for Next-generation Energy Storage Devices

Nobuhiro Ogihara

*Report received on Feb. 6, 2016*

**ABSTRACT** An intercalated metal-organic framework (iMOF) consisting of 2,6-naphthalene dicarboxylate dilithium (2,6-Naph$(COOLi)_2$) is introduced as a novel electrode material for energy storage devices. This material has a characteristic organic-inorganic layered crystalline structure comprising π-stacked naphthalene packing and tetrahedral $LiO_4$ units. The 2,6-Naph$(COOLi)_2$ undergoes a two electron-transfer reaction with a flat plateau at a potential of 0.8 V vs. $Li/Li^+$ and shows a very small change in unit-cell volume (0.33%) while maintaining the framework during Li intercalation. This volume strain reflects durability and is one order of magnitude lower than conventional intercalation electrode materials. The specific capacity and internal resistance of 2,6-Naph$(COOLi)_2$ can be improved through ordering of the π-stacked naphthalene packing with heat treatment. The operating potential of the proposed iMOF negative electrode leads to the following features in energy storage devices: a reduction of safety risk with lithium plating and a high-voltage bipolar battery configuration due to the common use of Al current collectors for bipolar electrodes.

**KEYWORDS** Energy Storage Devices, Carboxylates, Electrochemistry, Intercalations, Metal-organic Frameworks

## 1. Introduction

In rechargeable lithium-ion batteries for large-scale application, improvements in both battery and safety performance are required, and an electrode material with an appropriate operating potential is important for both. Basically, there have been two types of intercalation electrode materials for practical use, namely, lithium transition metal oxides[1,2] and graphite carbons.[3] With respect to electrochemical reversibility, which affects the cycle performance of an actual battery, intercalation electrode materials are of benefit because they undergo less severe volumetric changes of the main structure during cycling. As shown in **Fig. 1**(a), lithium transition metal oxides, which form layered, spinel, or olivine crystal structures, operate at potentials ranging from 1.5 to 5.0 V (vs. $Li/Li^+$). Graphite, which forms a layered structure with graphene-stacking, operates around 0.1 V. Although negative electrodes operating in actual battery cells at a low potential provide a wide cell voltage, which is determined by the potential difference between the positive and negative electrodes, there is a safety risk due to the lithium deposition, which can cause an internal short circuit between the positive and negative electrodes. Lithium titanate spinel ($Li_4Ti_5O_{12}$) operating at a potential of 1.55 V has previously been proposed as an alternative negative electrode material.[4] When lithium titanate is used, however, the cell voltage and total energy density become very low as a result. Layered $LiMS_2$ (M = Ti, V) sulfides with redox couples of $Ti^{3+}/Ti^{2+}$ and $V^{3+}/V^{2+}$, which give flat plateaus at about 0.5 and 1.0 V, respectively, have been proposed.[5] However, the capacities of these materials decrease during cycling due to a 30% volumetric change during charge and discharge. We therefore strongly believe that it is desirable to operate negative electrodes in the potential range of 0.5-1.0 V to minimize volumetric changes during cycling. Furthermore, because there are no Li-Al alloy reactions at potentials over 0.4 V, the target electrode materials can use Al current collectors, and high-voltage bipolar batteries can be constructed using Al current collectors for both the positive and the negative electrodes (Fig. 1(b)).

Under these circumstances, we focused on redox systems of π-conjugated aromatic dicarboxylate materials, which operate at potentials from 0.8 to 1.4 V.[6,7] We found that some of the resulting materials have a characteristic layered crystalline structure that maintains the framework during cycling. Herein, we present intercalation electrode materials utilizing

 

metal-organic frameworks (iMOFs) operated at a target potential of 0.8 V, as shown in Fig. 1(a). MOFs are crystalline materials that are composed of extended networks of metal ions connected by functionalized organic links to form three-dimensional networks.[8,9] In this paper, 2,6-naphthalene dicarboxylate dilithium (2,6-Naph(COOLi)$_2$) (**Fig. 2**(a)) is introduced as a representative iMOF electrode material for next-generation energy storage devices.[10-12]

## 2. Characterization of Intercalated Metal-organic Framework

2,6-Naph(COOLi)$_2$ was synthesized under reflux conditions in methanol by proton exchange reaction with lithium hydroxide monohydrate and 2,6-naphthalenedicarboxylic acid. An X-ray powder diffraction (XRD) pattern and the corresponding Rietveld refinement of the pristine sample confirmed that the 2,6-Naph(COOLi)$_2$ forms organic and inorganic layered crystalline structures in the *a*-axis direction comprising π-stacked naphthalene packing and tetrahedral $LiO_4$ network units, respectively (Fig. 2(a)). The tetrahedral $LiO_4$ units are framed by four O atoms of different naphthalene dicarboxylate units. This three-dimensional interaction provides almost complete insolubility in common organic electrolytes and thermal stability up to 800 K (527°C) (Fig. 2(b)).

Because 2,6-Naph(COOLi)$_2$ has a high thermal stability up to 800 K, the sample powder was annealed at temperatures between 523 and 723 K for 12 h under an Ar atmosphere. As shown in Fig. 2(c), the product was a white or gray powder. No color changes were observed when comparing pristine and heated samples at annealing temperatures of 523-673 K. In contrast, color changes from white to grayish-white were confirmed above 673 K, indicating carbonization.

**Figure 3** shows the dependence of the main XRD patterns of pristine and heated 2,6-Naph(COOLi)$_2$ for the (011) (Fig. 3(a)) and (102) (Fig. 3(b)) reflections, which correspond to the patterns of inorganic tetrahedral $LiO_4$ (Fig. 3(c)) and organic π-stacked naphthalene packing (Fig. 3(d)), respectively. There is a no 2$\theta$ position shift of the (011) reflection upon annealing (Fig. 3(a)); therefore, the structure of the inorganic unit is not affected by annealing. In contrast, the (102) reflection shifted to higher 2$\theta$ positions and decreased the full width at half maximum (Fig. 3(b)) upon annealing. For a pristine sample and a sample annealed at a low temperature of 523 K, two wide peaks were observed. This implies that several types of naphthalene packing and disordered structures exist. At annealing temperatures above 573 K, a single peak with a positive shift was observed, indicating densely ordering of the π-stacked naphthalene packing units. These results suggest that annealing improves the organic naphthalene packing ordering with no change in the inorganic $LiO_4$ network unit.

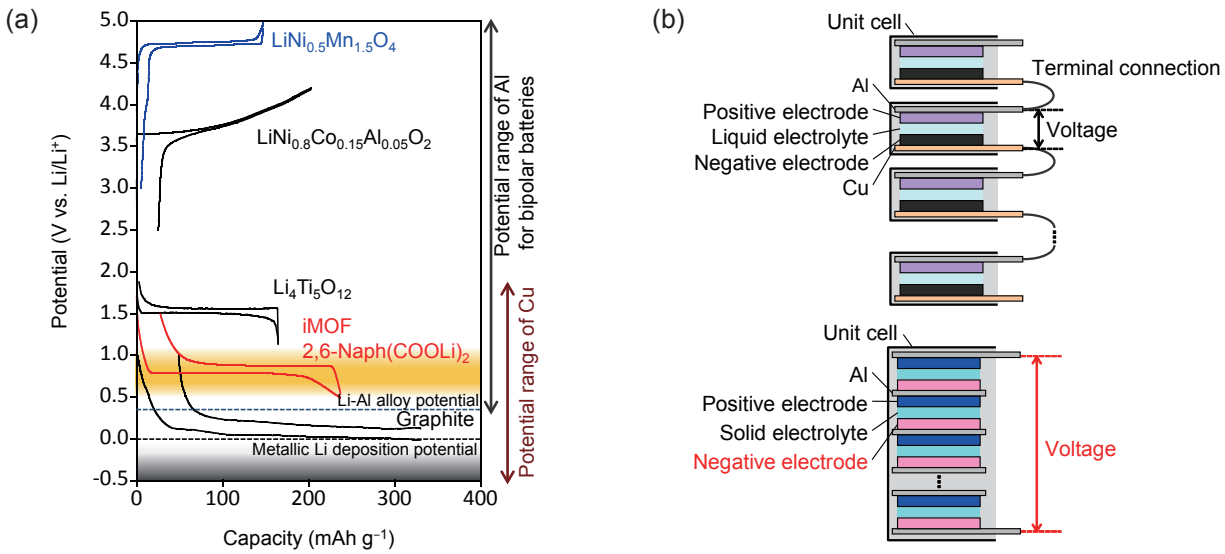


**Fig. 1** (a) Comparison of the electrode charge-discharge curves of the iMOF, 2,6-Naph(COOLi)$_2$, with those of other possible positive and negative intercalation electrodes with the effective potential ranges of Al and Cu current collectors. (b) Li-ion batteries connected in series (top) and proposed high-voltage bipolar Li-ion batteries (bottom).

 

## 3. Electrochemical Behavior

**Figure 4**(a) shows charge-discharge curves of Li/2,6-Naph(COOLi)$_2$ cells using pristine and annealed samples at various temperatures. All cells showed a flat plateau at a potential of 0.7 V. As shown in the inset of Fig. 4(a), the reversible capacities of the annealed samples were ca. 20 mAh g$^{-1}$ higher than that of the pristine sample, and the sample annealed at 623 K had the highest reversible capacity. In contrast, samples annealed above 673 K had slightly lower specific capacities than samples annealed below 623 K. As shown by the differential capacity *dQ/dV* plots in Figs. 4(b) and (c), the potential peak difference between the discharge and charge processes, which suggests that the polarization is due to the internal resistance of the electrode active materials for Li intercalation, decreased upon increasing the annealing temperature to 623 K, and increased for samples annealed above 673 K. Thus, the annealing of samples decreases the internal resistance, and the samples annealed at 573 and 623 K had the lowest internal resistance. This trend is similar to that observed for reversible capacity. Therefore, samples annealed at 573-623 K have a suitably high reversible capacity as well as a low internal resistance.

Comparing the reversible capacity and lattice constant of the unit cell, the reversible capacity showed a correlation with changes in the lattice parameter of the *c*-axis (**Fig. 5**(a)). The lattice parameter of the *c*-axis corresponds to the (102) reflection, i.e., the direction of the π-stacked naphthalene packing (Fig. 3(d)). A similar trend was confirmed with respect to both the reversible capacity and the inverse of the IV resistance

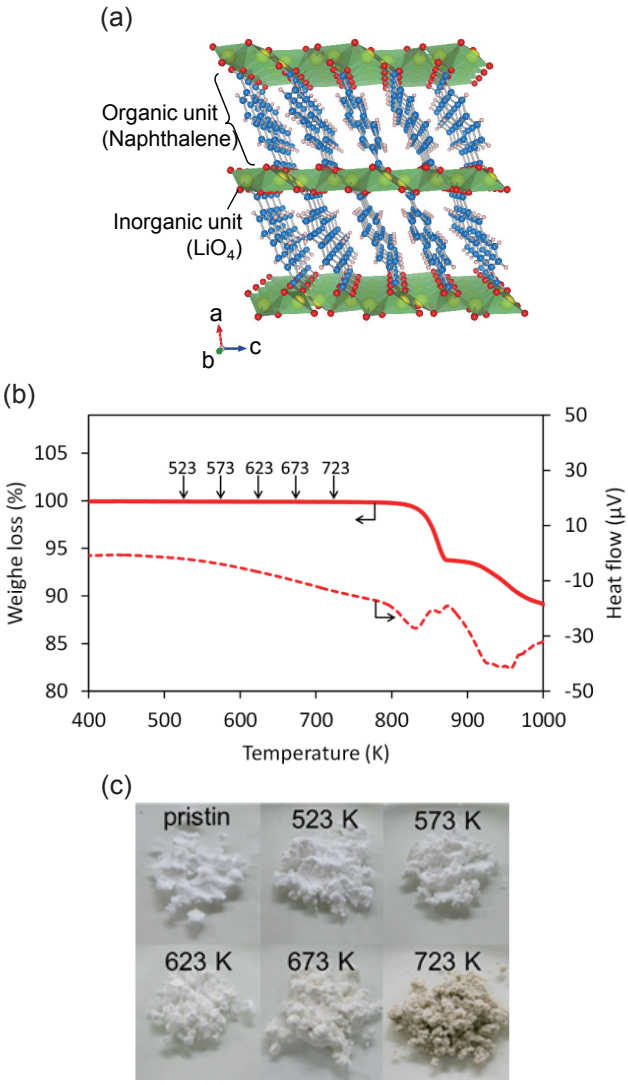


**Fig. 2** (a) Structure of a pristine sample taken, according to its XRD pattern (Li = yellow, O = red, C = blue, and H = white). (b) TG-DTA analysis of 2,6-Naph(COOLi)$_2$ and (c) photographs of pristine and annealed samples.

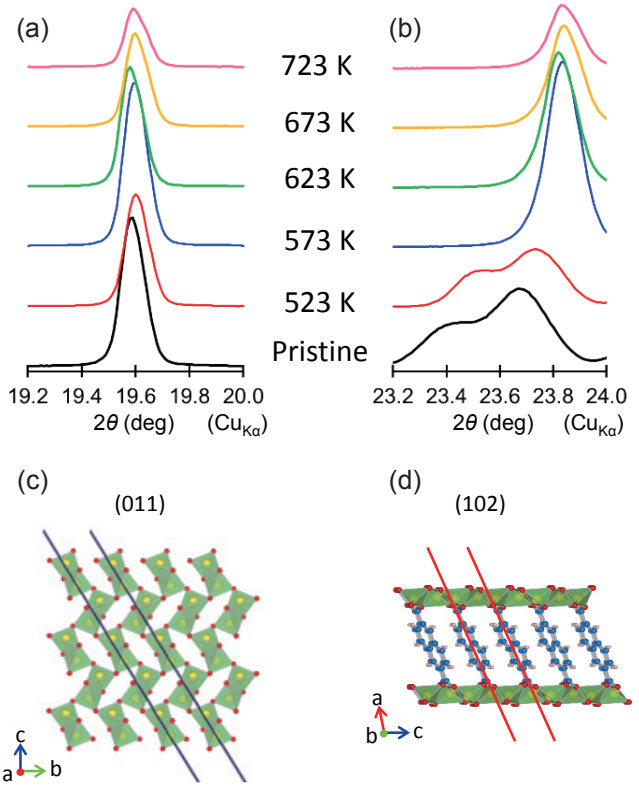


**Fig. 3** Powder XRD patterns for main reflections of (a) (011) and (b) (102) planes for pristine and annealed 2,6-Naph(COOLi)$_2$ samples, and schematic illustrations of the (c) (011) plane of the inorganic unit of the tetrahedral $LiO_4$ network and the (d) (102) plane of the organic unit of π-stacked naphthalene packing.

(Fig. 5(b)), which were highest for the sample annealed at 573 K. In contrast, the length of the *c*-axis decreases with increasing annealing temperature, but remains relatively constant for annealing temperatures greater than 573 K. This indicates that the reversible capacity increases and the internal resistance decreases because of the formation of an efficient electron and $Li^+$ pathway in the framework by narrowing the π-stacked naphthalene interlayer distance through ordering. Samples annealed at temperatures above 573 K become redox inert, partially because they begin to carbonize, as is evident in the pictures of annealed samples shown in Fig. 2(c).

For Li/2,6-Naph(COOLi)$_2$ cells based on optimized electrode material samples, as shown in **Fig. 6**(a), the discharge capacities for the first and second cycles were 360 and 220 mAh $g^{-1}$, respectively. The reversible capacity indicates an approximately two-electron transfer reaction, which corresponds to the theoretical capacity of 2,6-Naph(COOLi)$_2$, and is maintained after the second cycle (inset in Fig. 6(a)). To understand the Li intercalation mechanism, ex situ XRD analyses of 2,6-Naph(COOLi)$_2$ electrodes were performed during the first discharge and charge cycles (Fig. 6(b)). The

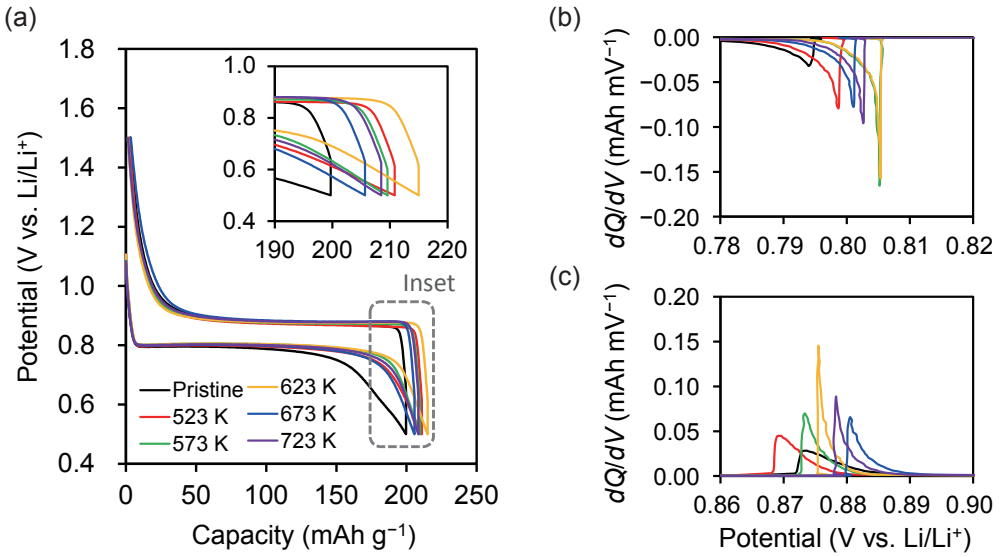


**Fig. 4** Comparison of the (a) charge-discharge curves, inset: end of the discharge curves for a Li/2,6-Naph(COOLi)$_2$ cell using pristine 2,6-Naph(COOLi)$_2$ and samples annealed at various temperatures. Differential capacity *dQ/dV* plots of (b) the discharge and (c) charge processes, which were calculated from the data shown in Fig. 4(a). The composition of the electrode was active material, carbon black, carboxy methyl cellulose, and styrene butadiene rubber (77.7:13.7:5.5:3.2 weight ratio, respectively).

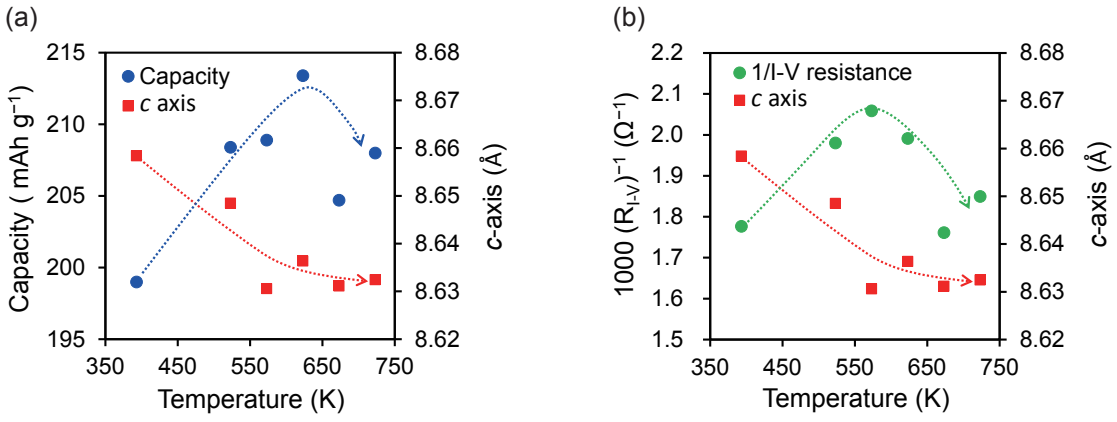


**Fig. 5** (a) Changes in the specific capacities and (b) the inverse of the IV resistance, and the lattice parameter of the *c*-axis as a function of annealing temperature. The IV resistance was calculated from the data of the polarization (*V*) obtained from the potential peak gap of the difference capacity *dQ/dV* plots shown in Figs. 4(b) and (c), and the measured current (*I*).

 

ex situ XRD patterns indicate a fully reversible redox process. The flat plateau profile and the evolution of the XRD patterns suggest that a two-phase reaction, $C_{10}H_6(COOLi)_2 \leftrightarrow C_{10}H_6(COOLi_2)_2$, occurs.

## 4. Detailed Lithium Intercalation Mechanism

The detailed crystal structure of this sample during Li intercalation was estimated from the XRD pattern and the corresponding Rietveld refinement obtained for a discharged sample. The results of the Rietveld refinement indicate that the layered framework of this sample was maintained during Li intercalation. Interestingly, the unit cell volume expands slightly after Li intercalation (+0.33%). As shown in **Fig. 7**, this value is one order of magnitude lower than that of Li-intercalated electrode materials such as graphite carbon materials,[13] $LiNiO_2$,[14] $LiCo_{1/3}Ni_{1/3}Mn_{1/3}O_2$,[15] $Li_2MnO_3$-$LiCo_{1/3}Ni_{1/3}Mn_{1/3}O_2$,[16] $Li_2Ru_{1-y}Sn_yO_3$,[17] $LiNi_{0.5}Mn_{1.5}O_4$ spinel,[18] $LiFePO_4$, or $A_2FePO_4F$ (A = Na, Li),[19] and is comparable to that observed for $Li_4Ti_5O_{12}$, (ca. 0.3%).[20,21] Moreover, this change in volume is much lower than that of the previously reported Fe-based MOF electrodes such as $Li_xK_{0.14}Mn_{1.43}[Fe^{III}(CN)_6]$[22] or $Fe^{III}(OH)_{0.8}F_{0.2}[O_2C\text{-}C_6H_4\text{-}CO_2]$.[23,24]

Detailed structural analysis indicated that there are two models for the Li intercalation state, as shown in **Fig. 8**. Model 1 shows that the intercalated $Li^+$ ions form a distorted tetrahedral $LiO_3C$ structure in their respective layers (Fig. 8(a)). The coordination structure near the intercalated $Li^+$ (Fig. 8(c)) suggests that the naphthalene C atom of a covalently bonded carboxylate group with a negative charge ($C^{\delta-}$) contributes to the $Li^+$- $C^{\delta-}$ interaction through an inductive effect of the carboxylate group. This tetrahedral $LiO_3C$ network may be primarily responsible for the Li conduction pathways into the bulk crystal. In contrast, Model 2 (Fig. 8(b)) shows that the intercalated $Li^+$ is located inside the π-stacked naphthalene packing, which indicates electrochemical doping of the Li into the π-stacked naphthalene layer (Fig. 8(d)). This leads to electronic conduction through the formation of an electron donor/acceptor complex.[25-28] Thus, the metal-organic framework of this material with a very small volume strain and efficient electron and $Li^+$ transport during Li intercalation leads to the observed electrochemical reversibility and small polarization.

## 5. Battery Performance with Intercalated Metal-organic Framework Electrodes

A 4 V single cell was fabricated with 2,6-Naph$(COOLi)_2$ negative and high operating potential $LiNi_{0.5}Mn_{1.5}O_4$[18,29,30] positive electrodes (Fig. 1(a)). The resulting charge-discharge test (inset

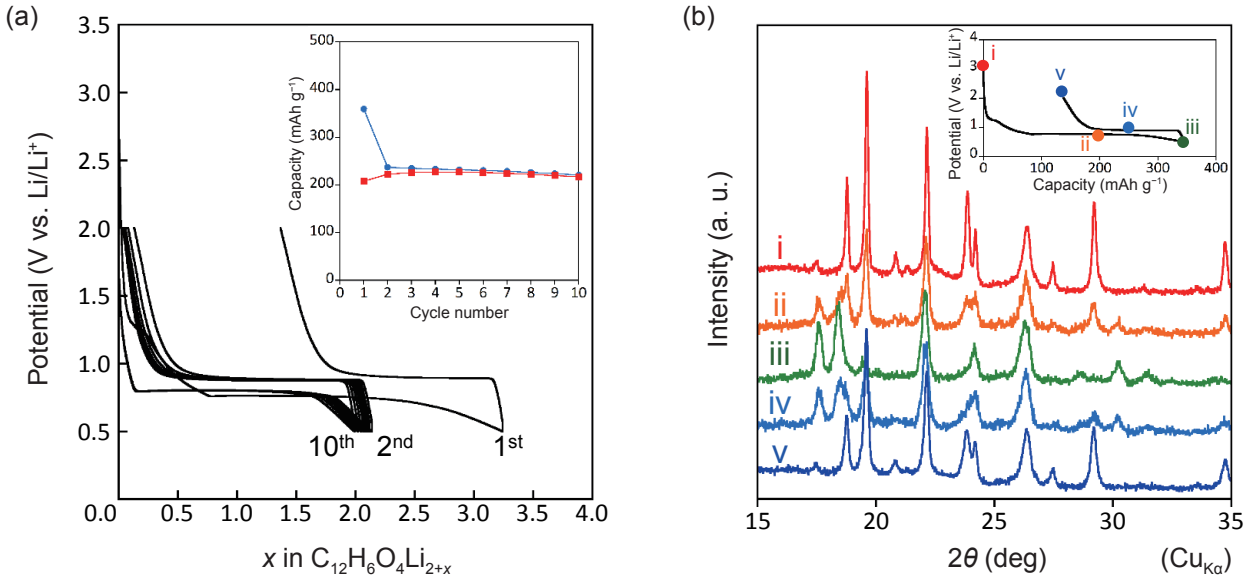


**Fig. 6** (a) Potential-composition profile for a Li/2,6-Naph$(COOLi)_2$ cell. Inset: corresponding discharge (circles) and charge (squares) capacities versus cycle number for the same cell. (b) XRD patterns for the Li/2,6-Naph$(COOLi)_2$ cell at various stages of the intercalation/deintercalation reaction. The composition of the electrode was active material, carbon black, vapor-grown carbon fiber, and polyvinylidene fluoride (66.7:11.1:11.1:11.1 weight ratio, respectively).

 

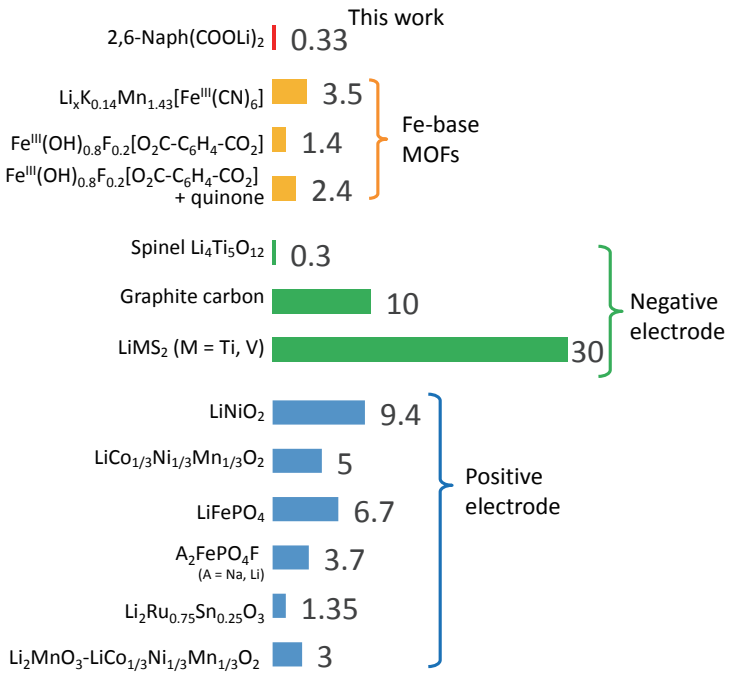


**Fig. 7** Comparison of the changes in volume during redox reactions.

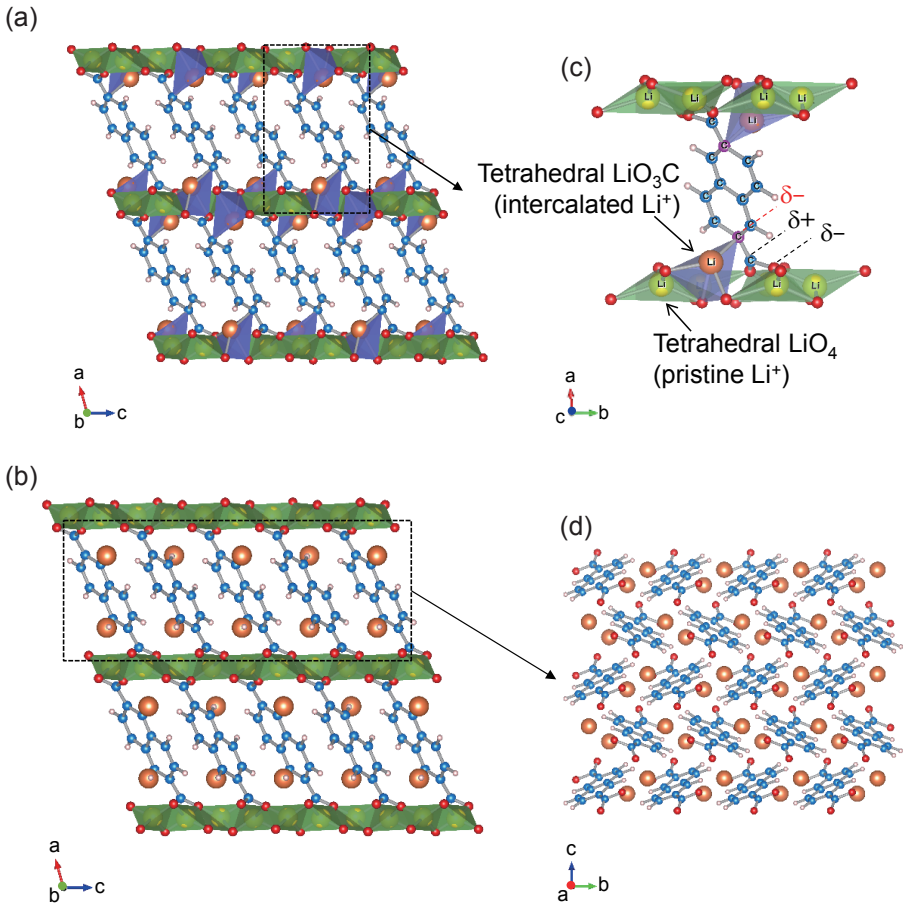


**Fig. 8** (a, b) The structure after Li intercalation in model 1 (a) and model 2 (b) viewed along the *b*-axis direction. (c, d) The coordination geometry near the intercalated $Li^+$ ions in model 1 (c) and the structure of Li-doped π-stacking naphthalene rings in model 2 (d).

 

of **Fig. 9**(a)) demonstrates a cell voltage of 3.9 V and a reproducible reversible capacity (Fig. 9(a)). As shown in Fig. 9(b), when using an Al current collector for both electrodes, the resulting discharge rate performance reveals that the proposed cells have a significantly higher specific energy (300 Wh $kg^{-1}$) than the previously reported 3 V Li-ion battery with $Li_4Ti_5O_{12}/LiNi_{0.5}Mn_{1.5}O_4$ cells (200 Wh $kg^{-1}$)[31] because of the higher cell voltage. Furthermore, the cells demonstrate a high specific power (100 Wh $kg^{-1}$) of about 5 kW $kg^{-1}$, comparable to current electric double-layer capacitors[32] or $Li_4Ti_5O_{12}$/activated carbon cells,[33,34] Si radical/graphite cells,[32] or nano-$TiO_2$-B/activated carbon cells,[35] which are candidates for high power storage applications. Using a gel-polymer electrolyte, we fabricated two-stack bipolar 2,6-Naph$(COOLi)_2/LiNi_{0.5}Mn_{1.5}O_4$ cells (**Fig. 10**(a)), successfully constructing an 8 V bipolar cell by connecting only two cells in series in a single pack (Fig. 10(b)).

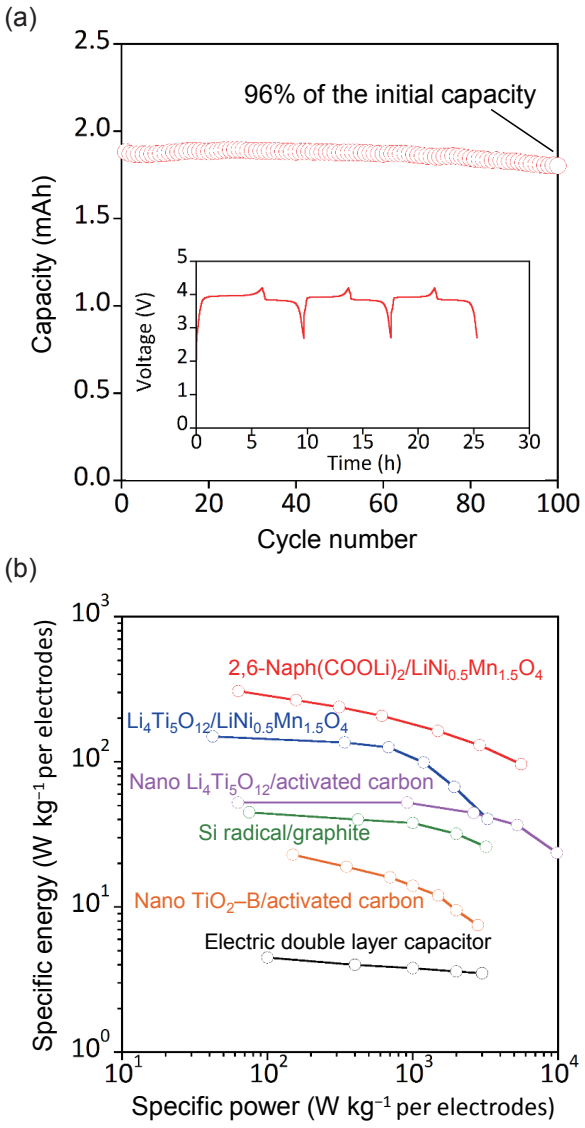


**Fig. 9** (a) Discharge capacities versus cycle number of a 2,6-Naph$(COOLi)_2/LiNi_{0.5}Mn_{1.5}O_4$ cell. Inset: charge-discharge curves of the same cell. (b) Comparison of specific energy versus specific power plots of the stackable cell composed of a negative electrode operating at more than 0.5 V (versus $Li/Li^+$).

## 6. Conclusions

In summary, we have demonstrated that an iMOF (2,6-Naph$(COOLi)_2$) electrode material has a desirable operating potential of 0.5-1.0 V for high voltage bipolar Li-ion batteries, along with a reversible Li intercalation mechanism. The iMOF electrode material also maintains its framework structure and is accompanied by a remarkably small volume change during Li

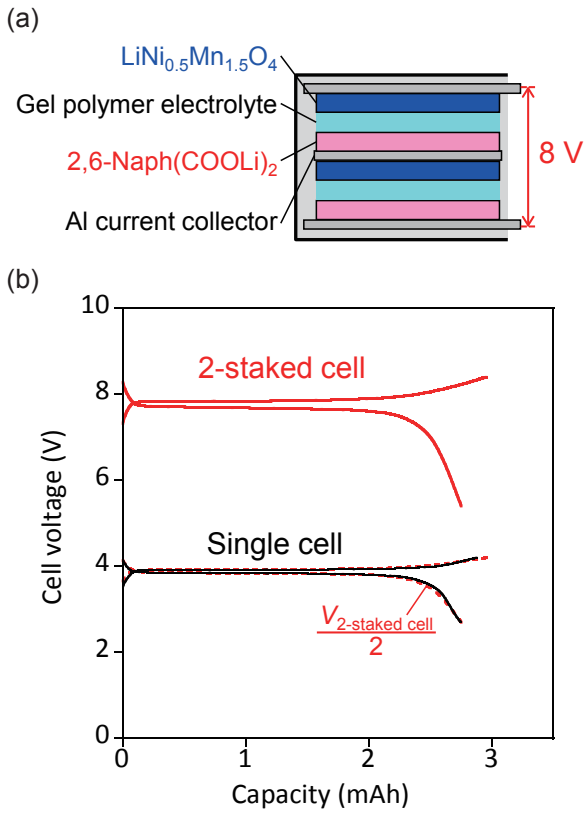


**Fig. 10** (a) Illustration of the prepared two-stacked 2,6-Naph$(COOLi)_2/LiNi_{0.5}Mn_{1.5}O_4$ bipolar cell. (b) Charge-discharge curves of single and two-stacked bipolar 2,6-Naph$(COOLi)_2/LiNi_{0.5}Mn_{1.5}O_4$ cells using a PVdF-HFP-based gel-polymer electrolyte. The dotted line shows the half voltage of the two-stacked bipolar cell.

 

intercalation with both electron and $Li^+$ transport by molecular self-assembly, and thus provides a favorable cycle stability. The practical application of iMOFs will aid in the design of high energy density batteries with improved safety. Thus, iMOFs will play an important role as negative electrodes in next-generation energy storage devices.

## Acknowledgements

The author thanks Prof. H. Uekusa of Tokyo Institute of Technology for powder XRD analysis. This study was performed in cooperation with member of Toyota Central R&D Labs., Inc. of Mr. Y. Kishida for powder XRD analysis, Dr. R. Ashahi, Dr. N. Ohba and Mr. K. Miyamoto for first-principles calculations, Dr. T. Ohsuna for TEM observations, and Ms. T. Yasuda for measuring the electrochemical behaviors. We also received support from Mr. T. Okuda for preparing of the bipolar cell, Mr. M. Shiozawa for SEM observations, and Dr. T. Sasaki for fruitful discussions.

## References

(1) Whittingham, M. S., "Lithium Batteries and Cathode Materials", *Chem. Rev*., Vol. 104, No. 10 (2004), pp. 4271-4301.
(2) Ariyoshi, K. and Ohzuku, T., "Conceptual Design for 12 V 'Lead-free' Accumulators for Automobile and Stationary Applications", *J. Power Sources*, Vol. 174, No. 2 (2007), pp. 1258-1262.
(3) Dahn, J. R., Zheng, T., Liu, Y. and Xue, J. S., "Mechanisms for Lithium Insertion in Carbonaceous Materials", *Science*, Vol. 270, No. 5236 (1995), pp. 590-593.
(4) Ohzuku, T., Ueda, A. and Yamamoto, N., "Zero-strain Insertion Material of $Li[Li_{1/3}Ti_{5/3}]O_4$ for Rechargeable Lithium Cells", *J. Electrochem. Soc*., Vol. 142, No. 5 (1995), pp. 1431-1435.
(5) Kim, Y., Park, K.-S., Song, S.-H., Han, J. and Goodenough, J. B., "Access to $M^{3+}/M^{2+}$ Redox Couples in Layered $LiMS_2$ Sulfides (M = Ti, V, Cr) as Anodes for Li-ion Battery", *J. Electrochem. Soc*., Vol. 156, No. 8 (2009), pp. A703-A708.
(6) Armand, M., Grugeon, S., Vezin, H., Laruelle, S., Ribiere, P., Poizot, P. and Tarascon, J.-M., "Conjugated Dicarboxylate Anodes for Li-ion Batteries", *Nat. Mater*., Vol. 8, No. 2 (2009), pp. 120-125.
(7) Walker, W., Grugeon, S., Vezin, H., Laruelle, S., Armand, M., Wudl, F. and Tarascon, J.-M., "Electrochemical Characterization of Lithium 4,4′-tolane-dicarboxylate for Use as a Negative Electrode in Li-ion Batteries", *J. Mater. Chem*., Vol. 21, No. 5 (2011), pp. 1615-1620.
(8) Eddaoudi, M., Kim, J., Rosi, N., Vodak, D., Wachter, J., O'Keeffe, M. and Yaghi, O. M., "Systematic Design of Pore Size and Functionality in Isoreticular MOFs and Their Application in Methane Storage", *Science*, Vol. 295, No. 5554 (2002), pp. 469-472.
(9) Rosi, N. L., Eckert, J., Eddaoudi, M., Vodak, D. T., Kim, J., O'Keeffe, M. and Yaghi, O. M., "Hydrogen Storage in Microporous Metal-organic Frameworks", *Science*, Vol. 300, No. 5622 (2003), pp. 1127-1129.
(10) Ogihara, N., Yasuda, T., Kishida, Y., Ohsuna, T., Miyamoto, K. and Ohba, N., "Organic Dicarboxylate Negative Electrode Materials with Remarkably Small Strain for High-voltage Bipolar Batteries", *Angew. Chem. Int. Ed*., Vol. 53, No. 43 (2014), pp. 11467-11472.
(11) Yasuda, T. and Ogihara, N., "Reformation of Organic Dicarboxylate Electrode Materials for Rechargeable Batteries by Molecular Self-assembly", *Chem. Commun*., Vol. 50, No. 78 (2014), pp. 11565-11567.
(12) Ogihara, N. and Kishida, Y., "Improvement in the Electrochemical Properties of Intercalated Metal-organic Framework Electrode Materials by Controlling Crystal Growth", *Electrochemistry*, Vol. 83, No. 10 (2015), pp. 861-863.
(13) Dahn, J., Fong, R. and Spoon, M., "Suppression of Staging in Lithium-intercalated Carbon by Disorder in the Host", *Phys. Rev. B*, Vol. 42, No. 10 (1990), pp. 6424-6432.
(14) Ohzuku, T., Ueda, A. and Nagayama, M., "Electrochemistry and Structural Chemistry of $LiNiO_2$ (R3m) for 4 Volt Secondary Lithium Cells", *J. Electrochem. Soc*., Vol. 140, No. 7 (1993), pp. 1862-1870.
(15) Yabuuchi, N., Makimura, Y. and Ohzuku, T., "Solid-state Chemistry and Electrochemistry of $LiCo_{1/3}Ni_{1/3}Mn_{1/3}O_2$ for Advanced Lithium-ion Batteries", *J. Electrochem. Soc*., Vol. 154, No. 4 (2007), pp. A314-A321.
(16) Yabuuchi, N., Yoshii, K., Myung, S. T., Nakai, I. and Komaba, S., "Detailed Studies of a High-capacity Electrode Material for Rechargeable Batteries, $Li_2MnO_3$-$LiCo_{1/3}Ni_{1/3}Mn_{1/3}O_2$", *J. Am. Chem. Soc*., Vol. 133, No. 12 (2011), pp. 4404-4419.
(17) Sathiya, M., Rousse, G., Ramesha, K., Laisa, C. P., Vezin, H., Sougrati, M. T., Doublet, M. L., Foix, D., Gonbeau, D., Walker, W., Prakash, A. S., Ben Hassine, M., Dupont, L. and Tarascon, J.-M., "Reversible Anionic Redox Chemistry in High-capacity Layered-oxide Electrodes", *Nat. Mater*., Vol. 12, No. 9 (2013), pp. 827-835.
(18) León, B., Lloris, J. M., Vicente, C. P. and Tirado, J. L., "Structure and Lithium Extraction Mechanism in $LiNi_{0.5}Mn_{1.5}O_4$ after Double Substitution with Iron and Titanium", *Electrochem. Solid-state Lett*., Vol. 9, No. 2 (2006), pp. A96-A100.
(19) Ellis, B. L., Makahnouk, W. R., Makimura, Y., Toghill, K.

 

and Nazar, L. F., "A Multifunctional 3.5 V Iron-based Phosphate Cathode for Rechargeable Batteries", *Nat. Mater.*, Vol. 6, No. 10 (2007), pp. 749-753.
(20) Scharner, S., Weppner, W. and Schmid-Beurmann, P., "Evidence of Two-phase Formation upon Lithium Insertion into the $Li_{1.33}Ti_{1.67}O_4$ Spinel", *J. Electrochem. Soc*., Vol. 146, No. 3 (1999), pp. 857-861.
(21) Ronci, F., Reale, P., Scrosati, B., Panero, S., Albertini, V. R., Perfetti, P., Di Michiel, M. and Merino, J. M., "High-resolution In-situ Structural Measurements of the $Li_{4/3}Ti_{5/3}O_4$ 'Zero-strain' Insertion Material", *J. Phys. Chem. B*, Vol. 106, No. 12 (2002), pp. 3082-3086.
(22) Okubo, M., Asakura, D., Mizuno, Y., Kim, J.-D., Mizokawa, T., Kudo, T. and Honma, I., "Switching Redox-active Sites by Valence Tautomerism in Prussian Blue Analogues $A_xMn_y[Fe(CN)_6] \bullet nH_2O$ (A: K, Rb): Robust Frameworks for Reversible Li Storage", *J. Phys. Chem. Lett*., Vol. 1, No. 14 (2010), pp. 2063-2071.
(23) Ferey, G., Millange, F., Morcrette, M., Serre, C., Doublet, M.-L., Greneche, J.-M. and Tarascon, J.-M., "Mixed-valence Li/Fe-based Metal-organic Frameworks with Both Reversible Redox and Sorption Properties", *Angew. Chem. Int. Ed.*, Vol. 46, No. 18 (2007), pp. 3259-3263.
(24) De Combarieu, G., Morcrette, M., Millange, F., Guillou, N., Cabana, J., Grey, C. P., Margiolaki, I., Ferey, G. and Tarascon, J.-M., "Influence of the Benzoquinone Sorption on the Structure and Electrochemical Performance of the MIL-53(Fe) Hybrid Porous Material in a Lithium-ion Battery", *Chem. Mater*., Vol. 21, No. 8 (2009), pp. 1602-1611.
(25) Potember, R. S., Hoffman, R. C., Hu, H. S., Cocchiaro, J. E., Viands, C. A. and Poehler, T. O., "Electronic Devices from Conducting Organics and Polymers", *Polym. J*., Vol. 19, No. 1 (1987), pp. 147-156.
(26) Potember, R. S., Poehler, T. O. and Benson, R. C., "Optical Switching in Semiconductor Organic Thin Films", *Appl. Phys. Lett*., Vol. 41, No. 6 (1982), p. 548.
(27) Potember, R. S., Poehler, T. O., Rappa, A., Cowan, D. O. and Bloch, A. N., "A Reversible Field Induced Phase Transition in Semiconducting Films of Silver and Copper TNAP Radical-ion Salts", *J. Am. Chem. Soc*., Vol. 102, No. 10 (1980), pp. 3659-3660.
(28) Heintz, R. A., Zhao, H., Ouyang, X., Grandinetti, G., Cowen, J. and Dunbar, K. R., "New Insight into the Nature of Cu(TCNQ): Solution Routes to Two Distinct Polymorphs and Their Relationship to Crystalline Films That Display Bistable Switching Behavior", *Inorg. Chem*., Vol. 38, No. 1 (1999), pp. 144-156.
(29) Zhong, Q., Bonakclarpour, A., Zhang, M. and Dahn, J. R., "Synthesis and Electrochemistry of $LiNi_xMn_{2-x}O_4$", *J. Electrochem. Soc*., Vol. 144, No. 1 (1997), pp. 205-213.
(30) Ohzuku, T., Takeda, S. and Iwanaga, M., "Solid-state Redox Potentials for $Li[Me_{1/2}Mn_{3/2}O_4$ (Me: 3d-transition Metal) Having Spinel-framework Structures: A Series of 5 Volt Materials for Advanced Lithium-ion Batteries", *J. Power Sources*, Vol. 81-82 (1999), pp. 90-94.
(31) Lee, S. W., Yabuuchi, N., Gallant, B. M., Chen, S., Kim, B. S., Hammond, P. T. and Shao-Horn, Y., "High-power Lithium Batteries from Functionalized Carbon-nanotube Electrodes", *Nat. Nanotechnol*., Vol. 5, No. 7 (2010), pp. 531-537.
(32) Maruyama, H., Nakano, H., Nakamoto, M. and Sekiguchi, A., "High-power Electrochemical Energy Storage System Employing Stable Radical Pseudocapacitors", *Angew. Chem. Int. Ed*., Vol. 53, No. 5 (2014), pp. 1324-1328.
(33) Naoi, K., Ishimoto, S., Miyamoto, J.-I. and Naoi, W., "Second Generation 'Nanohybrid Supercapacitor': Evolution of Capacitive Energy Storage Devices", *Energy Environ. Sci*., Vol. 5, No. 11 (2012), pp. 9363-9373.
(34) Naoi, K., Ishimoto, S., Isobe, Y. and Aoyagi, S., "High-rate Nano-crystalline $Li_4Ti_5O_{12}$ Attached on Carbon Nano-fibers for Hybrid Supercapacitors", *J. Power Sources*, Vol. 195, No. 18 (2010), pp. 6250-6254.
(35) Aravindan, V., Shubha, N., Ling, W. C. and Madhavi, S., "Constructing High Energy Density Non-aqueous Li-ion Capacitors Using Monoclinic $TiO_2$-B Nanorods as Insertion Host", *J. Mater. Chem. A*, Vol. 1, No. 20 (2013), pp. 6145-6151.



**Nobuhiro Ogihara**
Research Fields:
- Electrochemistry
- Energy Storage Devices
Academic Degree: Ph.D.
Academic Societies:
- The Electrochemical Society of Japan
- The Electrochemical Society